Softening Kinetics in High Al and High Al-Nb-Microalloyed Steels

B. Pereda, Z. Aretxabaleta, and B. López

Double-hit torsion tests were performed in order to study the effect of high Al levels (up to 2 wt.%) and Nb microalloying (up to 0.07 wt.%) on the static softening kinetics of 0.2%C-2%Mn steels. The addition of 1%Al leads to a delay in the softening kinetics due to solute-drag effect, equivalent to that exerted by 0.027%Nb. For the 2%Al steels, at temperatures below 1000 °C, $\gamma \rightarrow \alpha$ phase transformation occurs after deformation, resulting in a larger retardation of the softening kinetics. At temperatures higher than 1000 °C, Nb in solid solution also contributes to the retardation of the static softening kinetics, and at lower temperatures NbC strain-induced precipitation leads to incomplete softening for the 1%Al steel, and to a complex interaction between softening, phase transformation, and NbC strain-induced precipitation for the 2%Al-Nb steels. The effect of Al on the static softening kinetics was quantified and introduced in a model developed in previous works for the prediction of the austenite microstructural evolution. In order to validate the results of the model, multipass torsion tests were carried out at conditions representative of hot strip and plate rolling mills. Model predictions show reasonable agreement with the results obtained at different deformation conditions.

1. Introduction

In recent decades TRIP-assisted steels have attracted increasing interest due to the good strength and ductility balance and excellent formability that they exhibit. These steels present a multiphase room microstructure consisting of ferrite, bainite, and a small fraction, ~10%, of high C-retained austenite, which during deformation transforms into martensite, leading to high uniform elongation levels. Nowadays, TRIP-assisted steels are produced directly in hot strip rolling mills or as cold-rolled material in continuous annealing lines. In order to obtain the desired room microstructure, complex cooling sequences on the run out table and coiler or two-step heat treatments after cold rolling are usually applied. In addition, these steels usually contain Si additions in the 1-2 wt.% range in order to help stabilize the required austenite levels. However, high Si additions also impair the surface quality of the hot-rolled steel and result in poor galvanisability, and as a consequence, partial or complete substitution by other elements, such as Al, has been suggested (Ref 1). Moreover, microalloying with Nb has been proposed as a tool to further increase the strength level of TRIP steels (Ref 2).

B. Pereda, Z. Aretxabaleta, and **B. López,** Department of Materials, CEIT and TECNUN (Univ. of Navarra), Pº de M. Lardizabal, 15, 20018 Donostia-San Sebastián, Basque Country, Spain. Contact e-mail: blopez@ceit.es.

Several studies on the microstructures and mechanical properties of CMnAl and CMnAlSi steels have been carried out, leading to results comparable to those obtained in Si-alloyed steels (Ref 3-5). However, much less information can be found regarding the effect of high Si and Al levels on the austenite hot working behavior, even if this is an essential step in the steel production process. In the case of HSLA steels, application of thermomechanical treatments during hot deformation, Conventional Controlled Rolling for instance, is widely used as a tool to enhance the final product's mechanical properties. For TRIP-assisted steels, Conventional Controlled Rolling has also been shown to lead to microstructural refinement and increased retained austenite volume fraction and stability (Ref 2, 6), and it can even help in reaching the target mechanical property levels without the application of additional heat treatments (Ref 7). However, in order to define optimized rolling sequences, the effect that the high-alloying levels present in TRIP-aided steels exert on the austenite microstructure evolution must be taken into account.

In the literature, there is evidence that high Si and Al levels can significantly affect hot working behavior. Poliak et al. (Ref 8) observed that Al additions in the 1-1.7% range can increase the stress levels and modify the austenite dynamic softening kinetics. Suikkanen et al. (Ref 9) studied the static softening behavior of several types of high-strength TRIP-aided steels and determined that high Al levels result in a higher retardation effect than Si on the static softening kinetics. In a previous work, we found that 1%Al addition resulted in retardation in the static recrystallization kinetics of CMn steels due to solute-drag effect, while 2%Al addition promoted $\gamma \rightarrow \alpha$ transformation at typical hot rolling temperatures leading to strong retardation in the softening kinetics (Ref 10). High Al levels have also been shown to lead to an increase in the non-recrystallization temperature (T_{nr}) and can affect the efficiency of Nb-microalloying addition (Ref 11). However, the

amount of experimental data is limited and there is still lack of quantitative models which take into account the effect of Al on the static softening kinetics and the recrystallized microstructures or on how Al can affect the Nb(C, N) strain-induced precipitation kinetics.

In this work, the effect of high Al additions in the 1-2% range on the static softening behavior of CMn and Nb-microalloyed steels was investigated. The effect of Al in solid solution on the austenite softening kinetics was quantified and implemented in a pre-existing austenite microstructure evolution model. The predictions of the model were compared with experimental results obtained from multipass torsion tests carried out at deformation conditions representative of plate and strip rolling mills.

2. Experimental Techniques

The chemical composition of the steels investigated is listed in Table 1. The steels were produced in a laboratory unit with C and Mn levels typical of TRIP-assisted steels. A base CMn steel and two high Al levels of 1 and 2% were considered. Moreover, some of the Al-alloyed steels were also microalloyed with Nb in the 0.03-0.07% range. In addition, one steel with a low Al level and microalloyed with 0.03%Nb (C2Mn1Nb3) was also considered as a reference for analyzing the Al effect on the strain-induced precipitation kinetics.

In order to characterize the softening and multipass deformation behavior of the steels, different types of torsion tests were carried out. Specimen geometry details can be found in (Ref 10, 11). In all cases, a soaking treatment of 1250 °C for 15 min was applied. The initial austenite grain size values obtained after this treatment are included in Table 1. It must be noted that for all the 2%Al steels a small amount of ferrite (∼2% for the Al2 steel and less than 1% for the Al2Nb steels) was present in the specimens quenched after soaking (Ref 10, 11). This can be attributed to the strong ferrite stabilizing effect of Al (Ref 1, 12). This small ferrite fraction is not expected to affect the austenite softening evolution after deformation.

In order to study the softening behavior of the steels investigated, double-hit torsion tests were carried out under isothermal conditions in the 900-1065 °C temperature range. In the tests, pass-strains of 0.2 and 0.35 and a strain rate of 1 s^{-1} were applied. More details related to test procedure can be found in (Ref 10). From the stress-strain curves the fractional softening was determined by the 2% offset method (Ref 13).

Additionally, multipass torsion tests were carried out at deformation conditions representative of hot strip and plate laboratory rolling schedules starting at 40- and 140-mm thickness, respectively. For strip rolling simulation, sequences with different deformation levels corresponding to the production of gage thicknesses of 6 and 3 mm were considered, while in the case of plate rolling, the deformation sequences were performed at two different end rolling entry temperature ranges.

From above tests some specimens were also water quenched after deformation in order to study microstructure evolution and the strain-induced precipitation process. Samples were prepared following standard procedures and examined by conventional optical microscopy (OM) and transmission electron microscopy (TEM) means. More information about characterization techniques is indicated in Ref 10, 11.

3. Results

3.1 Fractional Softening

Figure 1 shows the fractional softening obtained for the steels investigated after deformation at ε = 0.35. For the C2Mn2 (Fig. 1a), Al1 (Fig. 1b), and Al2 (Fig. 1d) steels, the softening curves follow a sigmoidal shape at all the temperatures and can be fitted to an Avrami-type equation:

$$X = 1 - \exp\left(-0.693\left(\frac{t}{t_{0.5}}\right)^n\right), \tag{Eq 1}$$

where X is the fractional softening corresponding to a time t, $t_{0.5}$ is the time to reach 50% fractional softening (s), and n is the Avrami exponent. As is usually reported in the literature (Ref 14), for the three steels the softening kinetics is retarded with decreasing deformation temperature. However, it must be noted that the retardation effect due to the temperature decrease is significantly enhanced for the Al2 steel. In addition, although for the C2Mn2 and Al1 steels an approximately constant Avrami exponent of $n \sim 0.85$ was obtained for all the temperatures investigated, in the case of the Al2 steel this value decreases significantly by decreasing the temperature, from $n \sim 0.7$ at 1065 °C to $n \sim 0.32$ at 925 °C.

For the Nb-microalloyed steels, Al1Nb3 (Fig. 1c), Al2Nb3 (Fig. 1e), and Al2Nb7 (Fig. 1f), at the highest temperature, 1065 °C, the data can also be fitted to an Avrami-type curve. However, at lower temperatures the softening does not complete in the range of interpass times investigated. For the three steels, after deformation at 1000 °C, a softening saturation at ∼85% level is observed. At 965, 925 and 900 °C, the softening rate decreases significantly and also shows a halt at 30-40% levels. This type of softening saturation, known as a *plateau*, is typically observed in the softening curves obtained for Nb-microalloyed steels at low temperatures (Ref 15), and it is usually associated to Nb(C,N) strain-induced precipitation. The figure also shows that in all the cases, except for the

Table 1 Composition of the steels investigated (wt.%)

| Steel	C	Si	Mn	P	S	Al	N	Nb	Ti	D_0, μm
C2Mn2	0.195	0.01	1.98	0.019	0.001	0.03	0.005	0.001	0.005	69 ± 4
Al1	0.210	0.01	2.04	0.018	0.001	1.06	0.005	0.001	0.001	100 ± 3
Al1Nb3	0.205	0.02	1.97	0.018	0.001	0.88	0.004	0.028	0.001	102 ± 4
Al2	0.200	0.02	1.99	0.018	0.001	2.01	0.005	0.001	0.001	65 ± 2
Al2Nb3	0.205	0.01	2.03	0.018	0.001	2.02	0.005	0.030	0.001	65 ± 2
Al2Nb7	0.220	0.02	2.08	0.020	0.001	2.11	0.007	0.071	0.001	56 ± 2
C2Mn1Nb3	0.205	0.23	1.02	0.002	0.001	0.03	0.005	0.029	0.001	87 ± 4
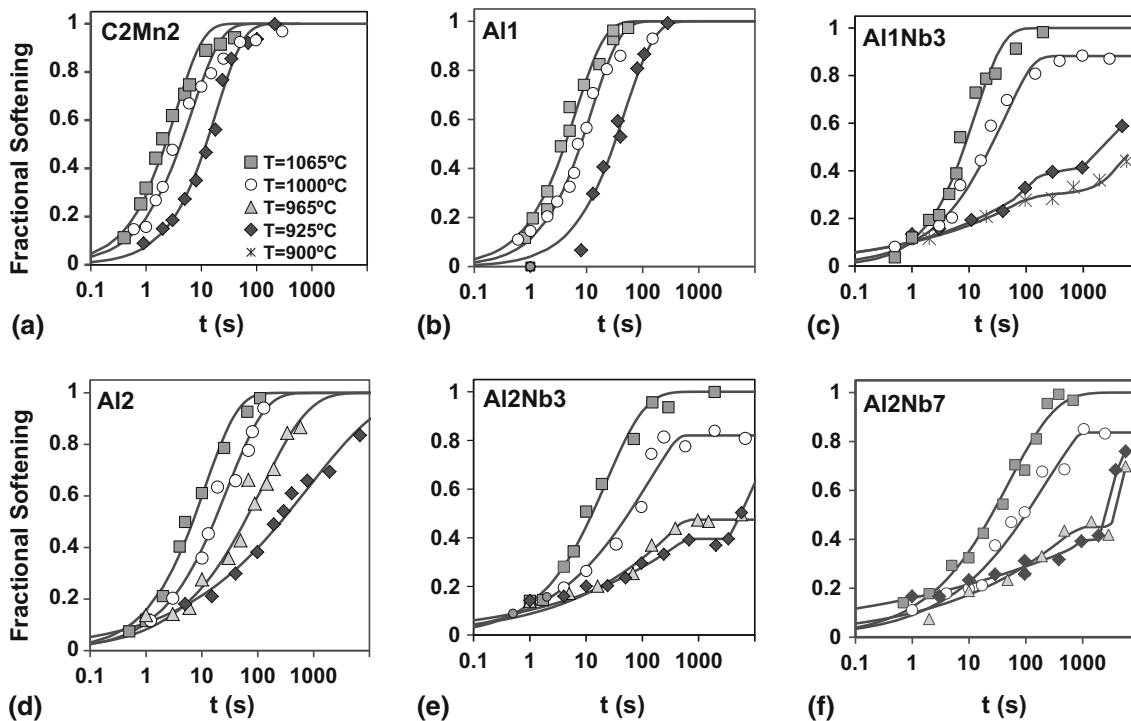
Fig. 1 Fractional softening obtained after deformation at different temperatures and ε = 0.35 for the steels investigated

Al2Nb3 steel at 965 °C, at longer interpass times the softening increases again.

The softening obtained for all the steels after deformation at temperatures of 1065, 1000, and 925 °C is compared in Fig. 2. Although the initial austenite grain size can affect the softening kinetics (Ref 16), the data obtained for the C2Mn2, Al2, and Al2Nb steels, and those corresponding to the Al1 and Al1Nb3 steels, can be directly compared as they show similar initial grain sizes of ∼65-69 μm for the first group of steels and ∼100 μm for the latter (see Table 1). As shown in Fig. 2(a), at the highest deformation temperature, 1065 °C, Al leads to a noticeable retardation in the softening kinetics, which is further enhanced by Nb addition. Similar trends are observed in Fig. 2(b), which corresponds to a deformation temperature of 1000 °C. As mentioned above, at this temperature the softening does not complete for the Nb-microalloyed steels. Finally, it is interesting to note that at the lowest temperature, 925 °C (Fig. 2c), the retarding effect due to 2% Al addition is significantly enhanced compared to 1% Al. In addition, the softening behavior obtained for the three Al-Nb steels is very similar, with softening levels that tend to saturate at ∼40% level and increase again at longer interpass times.

3.2 Microstructural Evolution During Softening

In a previous work, it was observed for the Al2 steel that at temperatures below 1000 °C, γ to α phase transformation took place after deformation, resulting in a significant softening delay which was also manifested by a decrease in the *n* Avrami exponent (Ref 10). In order to verify whether this behavior was followed by the rest of the steels, several specimens were quenched after deformation and different holding times for microstructural analysis. The results indicated that in the case of C2Mn2, Al1, and Al1Nb3, at all the temperatures, fully

austenitic microstructures developed during and after softening completion. For the Al2Nb steels, after deformation at 1065 °C the ferrite fraction also remained similar to the fraction present in the initial microstructure; however, at lower temperatures γ → α phase transformation was also found to occur concurrently with softening in these steels.

The ferrite fractions measured for all the 2%Al specimens at different conditions are summarized in Table 2, together with the softening levels corresponding to each test. It can be noted that in the case of the Al2Nb steels, the specimens selected for microstructural analysis were quenched at times corresponding approximately to the softening saturation start and finish times detected from the softening curves.

The table shows that for both Al2Nb steels, after deformation at 1000 °C and a holding time of $t = 576$ s, a ferrite fraction of $f_\alpha = 17\%$ was obtained, which is clearly larger than that present after reheating ($f_\alpha < 1\%$). Figure 3(a) and (b) shows the microstructure obtained for Al2Nb3 at these conditions, etched in 2%Nital and a picric acid solution, respectively. In Fig. 3(a), the ferrite grains can be clearly distinguished, aligned in bands parallel to the plastic flow direction. These can also be detected in Fig. 3(b), mainly located in the austenite grain boundaries (see black arrows). It must be noted that at 1000 °C the microstructure obtained for the Al2 steel at 95% softening conditions was mainly austenitic (Ref 10). Nevertheless, it should be taken into account that the time required to achieve a 95% softening for the Al2 steel, i.e., $t_{0.95} \sim 60$ s, is significantly shorter than the time corresponding to the beginning of the softening plateau in the Al2Nb steels, $t \sim 576$ s, where the microstructure is analyzed.

As shown in Table 2, at the lower temperatures of 965 and 925 °C, a significant ferrite fraction was detected in all the Al2Nb specimens. Figure 4(a) and (b) shows an example of the microstructures obtained for Al2Nb7 at 965 °C at the *plateau*
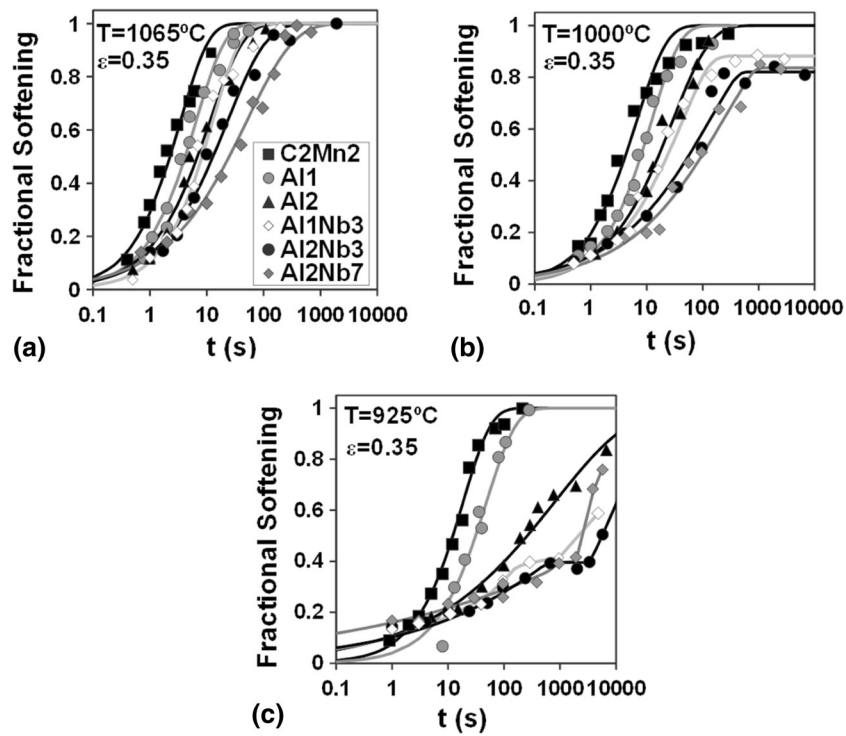
Fig. 2 Effect of steel composition on the softening determined after deformation at different temperatures

Table 2 Precipitate sizes, ferrite fraction (if present), and fractional softening corresponding to the 2%Al specimens quenched for metallographic analysis

| Steel	$D\gamma_0$, μm	T_{def}, °C	t_{ip}, s	f_α, %	FS, %	D_{prec}, nm γ	α
Al2	65	Initial microstructure		~2	...	...	...
		965	60	19	50	...	...
		925	0	1.3	0	...	...
			270	17	50	...	...
			404	24	55	...	...
			960	17	65	...	...
			2400	90	76	...	...
			10200	100	90	...	...
Al2Nb3	65	Initial microstructure		<1	...	93 ± 7	...
		1000	576	17	78	76 ± 19	151 ± 22
		965	384	32	43	30 ± 4	91 ± 12
		925	672	29	39	14 ± 1	18 ± 1
			5760	~100	50	24 ± 1	33 ± 1
Al2Nb7	56	Initial microstructure		<1	...	126 ± 6	...
		1000	576	17		60 ± 5	199 ± 31
		965	384	15	39	19 ± 1	20 ± 1
			5760	100	70	33 ± 1	42 ± 1
		925	672	30	36	18 ± 1	18 ± 1
			5760	100	76	...	30 ± 2
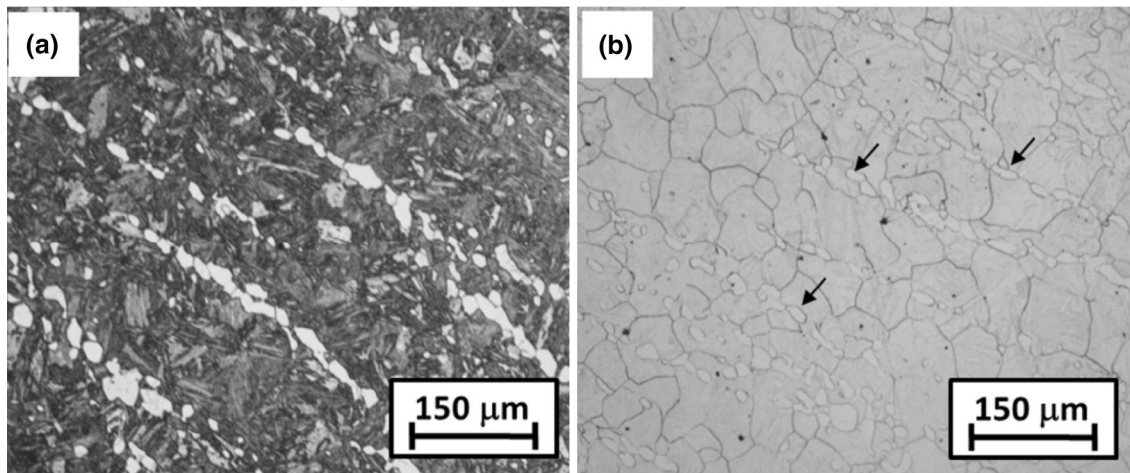
Fig. 3 Examples of the microstructures obtained for the Al2Nb3 steel after deformation at 1000 °C at the time for the plateau onset (t = 576, FS $\sim$ 80%, $f\alpha$ = 17%) after etching in (a) 2%Nital and (b) picric acid
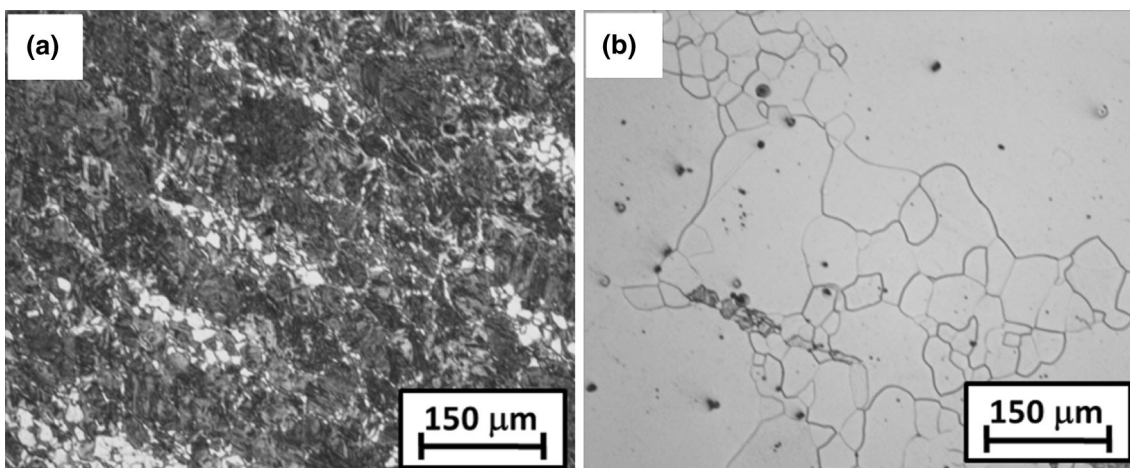

Fig. 4 Microstructures obtained after etching in 2%Nital for the Al2Nb7 steel after deformation at 965 °C at times corresponding to (a) t = 384 s, FS = 39%, $f\alpha$ = 15%, and (b) t = 5760 s, FS = 70%, $f\alpha \sim$ 100%

onset and end times, t = 384 s and t = 5760 s, respectively (2%Nital etching). At the beginning of the plateau (Fig. 4a), a ferrite fraction of f_α = 15% is present in the microstructure. This ferrite fraction increases as the holding time does until a nearly fully ferritic microstructure is reached (Fig. 4b). Note from the micrograph that some martensite islands remain, although the fraction is relatively low. Taking into account the high carbon content of the steel, a second phase of carbon-enriched retained austenite would be expected instead of martensite. Nevertheless, it seems that in contrast to theory, a high carbon content is remaining in solid solution in this ferrite. It is interesting to note that this ferrite has a significantly higher hardness than the ferrite present in the as-received laboratory hot-rolled material, where the microstructure consisted of ferrite-pearlite. This suggests that this ferrite formed at high temperatures is hardened by the high amount of carbon which seems to be retained in solid solution.

At the rest of conditions investigated, the results obtained for the two Al2Nb steels were similar; at times corresponding to the *plateau* onset the ferrite fractions ranged from 15 to 30%, while at the *plateau* finish times, almost fully ferritic microstructures were observed (see

Table 2). It is interesting to note that even in the cases where the microstructure was mainly constituted by ferrite, relatively low fractional softening levels, ranging from 50 to 70%, were determined. Above-mentioned ferrite hardening would also be contributing to obtain these low mechanical softening levels.

Phase transformation taking place after deformation for the Al2 and Al2Nb steels can be attributed to the high Al content of these steels (2 wt.%), which has been reported to be a strong ferrite stabilizer (Ref 1, 12, 17). This also agrees well with calculations performed with the Thermo-Calc software, which predicts that for these steels 1%Al leads to an increase in the A_{e3} temperature from 780 to 900 °C, while 2%Al results in a further increase up to 1030 °C (Ref 18, 19).

3.3 Strain-Induced Precipitation

In Nb-microalloyed steels, softening retardation can be due to the solute-drag effect exerted by Nb in solid solution, or to the pinning effect caused by strain-induced precipitates, the latter usually exerting the stronger effect (Ref 20, 21). For the high Al-Nb steels, in addition to Nb(C,N), the possibility of AlN
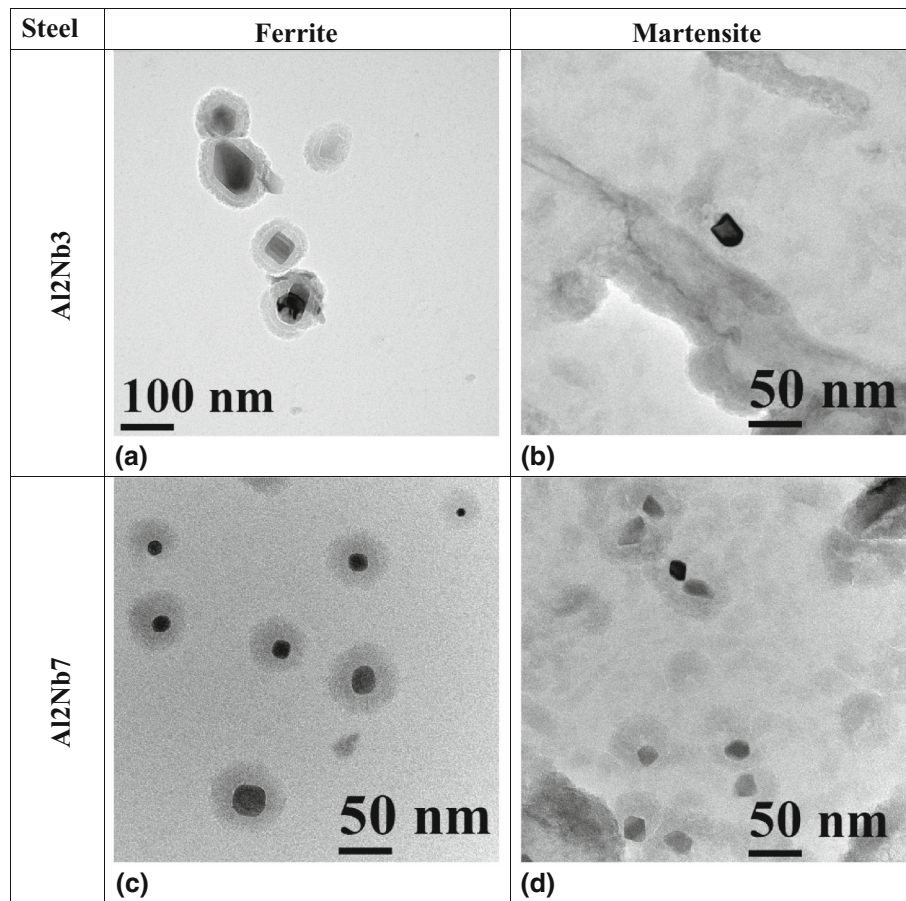
Steel	Ferrite	Martensite
Al2Nb3	100 nm (a)	50 nm (b)
Al2Nb7	50 nm (c)	50 nm (d)

Fig. 5 Precipitates extracted from the Al2Nb specimens quenched after deformation at 965 °C at times corresponding to the plateau onset ($t = 384$ s)

precipitation might be considered. However, in these steels the fraction of AlN which can be formed is limited by the N content ($\sim$50 ppm), and therefore, the amount of Al that can be engaged in the form of AlN is the same, and it is very small ($<$0.01 wt.%) for all the steels investigated (Ref 10). In addition, equilibrium calculations carried out with the Thermo-Calc software (Ref 18) indicate that the dissolution temperature of the AlN phase is higher than the soaking temperature employed in the tests, 1250 °C. The presence of very coarse undissolved Al- and N-bearing particles, larger than 1 μm, was confirmed by SEM analysis in Al1 and Al2 specimens quenched after soaking. Due to their coarse size, these particles are not expected to affect the softening behavior of the steels investigated, and therefore, an effect of Al in solid solution is only expected. Furthermore, another consequence of interest is that all the N content present in these steels is expected to be caught in the form of AlN, and as a result, strain-induced precipitation of Nb can only take place in the form of Nb carbides, which are expected to precipitate at lower temperatures than Nb nitrides and carbonitrides.

3.3.1 Al2Nb3 and Al2Nb7 Steels. As mentioned above, for the Al2Nb steels, as well as martensite (product of the quenched austenite), ferrite was detected in the specimens prepared for metallographic analysis. However, since the carbon extraction replicas reveal the topography of the etched samples, it was possible to easily distinguish the precipitates present in the two phases. The precipitate size measurements are summarized in Table 2.

For both steels, first the specimens quenched after soaking were examined in order to analyze the initial precipitation state. For the Al2Nb3 steel, although some Nb precipitates could be detected, these were very scarce. On the other hand, in the case of the Al2Nb7, a significant amount of relatively coarse precipitates with an average size of 126 nm were found. This indicates that for Al2Nb7, after reheating at 1250 °C, only part of the Nb-microalloying content was put into solution. This is in good agreement with the prediction of different solubility products found in the literature (Ref 22, 23).

Table 2 indicates that Nb-containing particles were also detected in all the specimens quenched after deformation. However, it must be mentioned that for Al2Nb3, at the highest temperature considered (1000 °C), the precipitates in the martensite regions were very scarce and relatively coarse, $D_{\text{prec}} = 76$ nm, which suggests a limited interaction of strain-induced precipitation with softening kinetics. For Al2Nb7, the number of particles was larger. Although the measured precipitate size, $D_{\text{prec}} = 60$ nm, was also relatively large, this is clearly finer than the size of the undissolved precipitates, 126 nm. This suggests that for the Al2Nb7 a certain amount of strain-induced precipitation has taken place at these conditions. After quenching at 1000 °C, the ferrite fraction present in the specimens was relatively low, $f_{\alpha} = 17\%$, whereas some Nb precipitates could also be detected in these areas, their size being significantly coarser than in the martensite, $D_{\text{prec}} = 151$ and 199 nm for the Al2Nb3 and Al2Nb7, respectively.

Table 3 Mean precipitate sizes measured at different conditions for the Al1Nb3 C2Mn1Nb3 steels

Steel	$D_{\gamma 0}$, μm	T_{def}, °C	ε	t, s	D_{prec}, nm
Al1Nb3	~102	1000	0.35	384	44 ± 7
		925		96	13 ± 1
				288	13 ± 1
				960	28 ± 1
				4800	20 ± 1
		900		96	7 ± 1
				960	14 ± 1
				5760	19 ± 1
C2Mn1Nb3	~87	925	0.35	58	9 ± 1
				4800	20 ± 1
		900		96	8 ± 1
				5760	16 ± 1

Some examples of precipitates extracted from both Al2Nb steels after deformation at a lower temperature of 965 °C and quenching at $t \sim 384$ s, the time at which the softening plateau begins, are shown in Fig. 5. The figure includes examples from both ferrite (Fig. 5a-c) and martensite (Fig. 5b and d) precipitates. From Fig. 5(a) and (b), it can be observed that, similar to 1000 °C, for the Al2Nb3 steel the precipitates were scarce, and significantly larger in ferrite, $D_{prec} = 91$ nm, than in martensite, $D_{prec} = 30$ nm. On the other hand, for Al2Nb7, (Fig. 5c and d), precipitates were more abundant and of similar size in the ferrite, $D_{prec} = 20$ nm, and martensite, $D_{prec} = 19$ nm. At the lowest temperature investigated, 925 °C, the results obtained were similar for both steels; the precipitates were very abundant, and of similar size in martensite ($D_{prec} = 14$ and 18 nm for Al2Nb3 and AlNb7, respectively) and in ferrite ($D_{prec} = 18$ nm for both steels).

As mentioned above, the microstructure obtained at longer interpass times (*plateau* end), was mainly fully ferritic in all the Al2Nb specimens analyzed. The precipitates detected at these conditions were larger and also more abundant than at shorter times, both in the ferrite regions and in the remaining martensite islands, denoting that precipitate growth and/or coarsening processes take place during isothermal holding time (see Table 2). For example, for the Al2Nb3 steel, after deformation at 925 °C, the precipitate size in the martensite regions increased from 14 to 24 nm, and in the case of the ferrite regions, from 18 to 33 nm.

3.3.2 C2Mn1Nb3 and Al1Nb3 Steels. In the case of the Al1Nb3 steel, the microstructure obtained after deformation was austenitic in all the cases and the strain-induced precipitation process could be investigated without interaction with phase transformation. In order to analyze the effect of Al on the strain-induced precipitation process, the results obtained for this steel were compared with the reference C2Mn1Nb3 steel, which shows a low Al level, 0.03%, and Nb and C contents similar to the Al1Nb3 steel (see Table 1). The conditions analyzed and precipitate sizes obtained for both steels have been summarized in Table 3.

After soaking, the amount of precipitates present in both steels was very scarce, denoting that nearly all the Nb was dissolved after reheating, which is in good agreement with the results of most solubility products found in the literature (Ref 22, 23). Similarly, after deformation at 1000 °C, the number of precipitates present at the time for the *plateau* onset ($t \sim 384$ s) was very scarce, and their size relatively large, 44 nm. This suggests that as in the case of the Al2Nb3 steel, the effect of strain-induced precipitation is limited at this temperature. On the other hand, at lower temperatures of 900 and 925 °C, a high amount of Nb precipitates was detected in all the specimens. Figure 6 shows several TEM micrographs taken from the replicas extracted after deformation at 900 °C for both steels at holding times of $t = 96$ and 5760 s. In both steels, the precipitate size tends to increase with increasing interpass time, which can be attributed to growth and/or coarsening processes taking place during isothermal holding. It can also be observed from Table 3 that the measured precipitate sizes were very similar for both steels. Nevertheless, it should be noted that at the shortest interpass time of $t \sim 96$ s, the amount of precipitates present in the C2Mn1Nb3 specimen was significantly higher than in the Al1Nb3 [compare Fig. 6(a) and (c)]. As shown in the figure, at larger interpass times, less difference is observed. Similar trends were found at a temperature of 925 °C. It must be noted that these differences in the precipitation state are also reflected in the softening behavior. At both 900 and 925 °C, the softening kinetics was delayed in the C2Mn1Nb3 steel compared to the Al1Nb3 steel, i.e., for a given holding time the softening fraction is always larger in the Al steel. This softening delay can be attributed to an enhanced pinning effect exerted by the precipitates in the Al-free steel. This suggests that Al could have a retardation effect on Nb precipitation kinetics.

3.4 Recrystallized Microstructure

The recrystallized microstructures were characterized in those cases where strain-induced precipitation or phase transformation did not take place, that is, for the Al2 steel at temperatures above 965 °C, for Al1Nb3, Al2Nb3, and Al2Nb7 at 1065 °C, and for the C2Mn2 and Al1 steels at all the temperatures investigated. The mean equivalent diameters measured at the different deformation conditions are summarized in Table 4. From the experimental data, no significant effect of temperature on the recrystallized grain size is observed. In contrast, decreasing the applied strain leads in all cases to an increase in the austenite grain size. This behavior is in concordance with that reported by other authors who have only found an effect of the initial grain size and strain, but none of temperature (Ref 24-26).

4. Discussion

4.1 Static Softening Kinetics

As seen above, in the absence of strain-induced precipitation, the experimental fractional softening data can be fitted reasonably to sigmoidal Avrami-type curves. Hence, the time for 50% fractional softening, $t_{0.5}$, can be described by the following empirical relationship (Ref 25):

$$t_{0.5} = A D_0^m \epsilon^{-p} \dot{\epsilon}^{-q} \exp\left(\frac{Q}{RT}\right), \quad \text{(Eq 2)}$$

where A, m, p, and q are material constants, Q is the activation energy for static recrystallization (J/mol), R is the gas constant (J/mol K), D_0 is the initial austenite grain size (μm), ϵ and $\dot{\epsilon}$ are the strain and strain rate (s^{-1}), and T is the deformation temperature (K). Knowledge of the dependence of
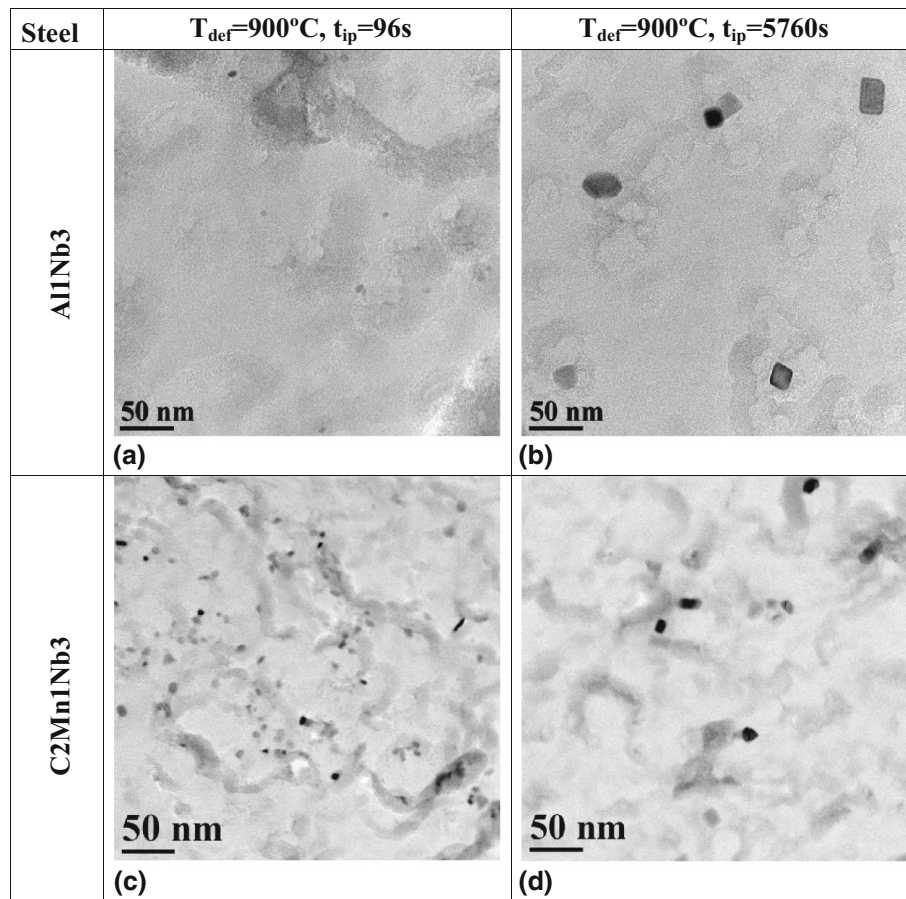
Fig. 6 Precipitation state evolution for the Al1Nb3 and C2Mn1Nb3 steels after deformation at 900 °C

Table 4 Recrystallized grain sizes measured for the steels tested in this work at different strain conditions

Steel	$D_{\gamma 0}$, µm	T_{def}, °C	ε	$D_{\gamma rex}$, µm
C2Mn2	69	1065	0.35	56 ± 2
		1065	0.2	67 ± 2
		925	0.35	63 ± 3
Al1	100	1065	0.35	62 ± 3
		1065	0.2	96 ± 5
		925	0.35	53 ± 2
Al2	65	1065	0.35	60 ± 2
		1065	0.2	68 ± 2
		1000	0.35	52 ± 2
Al1Nb3	102	1065	0.35	70 ± 3
Al2Nb3	65	1065	0.35	48 ± 1
Al2Nb7	56	1065	0.35	36 ± 1

Avrami exponent n and $t_{0.5}$ on the thermomechanical and metallurgical parameters allows a complete description of the softening kinetics.

For the C2Mn2 and Al1 steels, an approximately constant Avrami exponent with a calculated mean value of $n \sim 0.85$ was obtained, a value that was unaffected by pass-strain or deformation temperature. A similar value of $n \sim 0.87$ is obtained for the Al1Nb3 steel in the absence of interaction with strain-induced precipitation ($T = 1065$ °C). These values are slightly lower than those reported by Suikkanen et al.

(Ref 9), $n = 1.1$ to 1.4, who studied recrystallization kinetics for various Al- and Si-alloyed steels, with C and Mn contents similar to the present C2Mn2 steel, using stress relaxation tests. However, the present values are in the range of those reported for low carbon C-Mn and Nb, Nb-Ti-microalloyed steels in the absence of strain-induced precipitation, $n = 0.9$-1 (Ref 16, 27, 28). Although Medina et al. (Ref 29) have proposed a temperature dependence for the Avrami exponent, the values predicted by their model in the temperature range investigated, $n = 0.87$-0.95, are also similar to those obtained in this work.

For the 2%Al steels, lower n values were determined. For Al2 at 1065 °C, an exponent of $n = 0.73$ was obtained. In addition, a decrease in this exponent is observed with a temperature reduction, from $n = 0.73$ at 1065 °C to $n = 0.32$ at 925 °C. This was attributed to the effect of austenite to ferrite transformation during softening evolution. For the Nb-microalloyed steels, when interaction with precipitation and/or phase transformation occurs, low n values are also observed ($n \leq 0.6$). These values are in the range of those reported by Grajcar et al. for Al-Nb TRIP steels with Al levels up to 1.7 (Ref 30).

With respect to the dependence of $t_{0.5}$ on the different parameters and taking into account the limited amount of data, the relationships reported in the literature were assumed here. For the initial grain size, strain, and strain-rate dependence, the values proposed by Fernandez et al. were considered, i.e., a linear relationship with the initial grain size, $m = 1$, and $p = 5.6D_0^{-0.15}$ and $q = 0.53$ for the strain and strain-rate exponents, respectively (Ref 16). In order to study the effect

of Al and Nb addition, a normalized recrystallization time, $\tau_{0.5}$, which is independent of strain, strain rate, and grain size, was determined for all the tests as follows:

$$\tau_{0.5} = \frac{t_{0.5}}{D_0 \cdot \epsilon^{-5.6D_0^{-0.15}} \cdot \dot{\epsilon}^{-0.53}}. \qquad (Eq\ 3)$$

The $\tau_{0.5}$ values obtained for the different steels and deformation temperatures are plotted in Fig. 7. It can be noticed that both Al and Nb additions lead to a significant retardation in recrystallization time. However, the microstructural characterization indicates that the mechanisms responsible for the slower softening kinetics depend in each case on the steel composition and deformation temperature. It can be observed that the addition of 1 wt.%Al to the C2Mn2 reference steel results in a time delay at all the temperatures. This retardation can be attributed to Al solute-drag effect. The same can be said for the case of 2 wt.%Al addition above 1000 °C. In this temperature range, further addition of Nb enhances retardation since the solute-drag effect of Nb adds to that exerted by Al. At temperatures below 1000 °C, because of the interaction between softening and other phenomena, a more pronounced retardation is observed in Fig. 7, particularly for the Al2 and Al2Nb steels. For these steels, $\gamma \rightarrow \alpha$ phase transformation occurs concurrently with static softening and this leads to a strong retardation effect. This behavior can be attributed to the competition between recrystallization and phase transformation as both processes share the prior austenite grain boundaries as nucleation sites for recrystallized and ferrite grains. Therefore, early consumption of austenite grain boundaries by ferrite grains could prevent to some extent the occurrence of recrystallization. It must be mentioned that, as well as retarding the softening kinetics, phase transformation has been observed to lead to a significant increase of the T_{nr} and thus of the potential for strain accumulation during multipass deformation. However, it also led to a significant loss of hot-ductility, which limits the industrial applicability of the 2%Al steels (Ref 11).

When Nb is added, softening evolution becomes even more complex due to its interaction with phase transformation as well as strain-induced precipitation. In the Al2Nb steels, the combination of both mechanisms results in very long softening times or even a complete stop of softening, Fig. 7. As mentioned above, for the Al1Nb3 steel, strain-induced precipitation of Nb(C,N) particles appears to be the main mechanism responsible for softening retardation at the lowest temperatures of 925 and 900 °C.

In order to quantify the softening delay exerted by Al in solid solution, the solute retardation parameter (SRP) was calculated, excluding the conditions where precipitation or phase transformation takes place, as follows (Ref 31):

$$SRP = \ln\left(\frac{\tau_{0.5}}{\tau_{0.5REF}}\right) \times \frac{0.1}{wt.\%} \times 100\%, \qquad (Eq\ 4)$$

where $\tau_{0.5}$ is the normalized recrystallization time of the Al-alloyed steels (Al1, Al2, and Al2Nb3) and $\tau_{0.5REF}$ is the normalized time calculated for the reference steels (i.e., C2Mn2 for the first two steels and Al1Nb3 for the other steel).

In this work, an average value of SRP = 6 was obtained for Al, with no clear effect of deformation conditions or Al content within the range investigated. This value is lower than those of 16 and 38 reported for Al in C-Mn and Nb-microalloyed steels, respectively (Ref 32, 33). However, it must be taken into account that the Al content of these steels, ~0.08%, was more
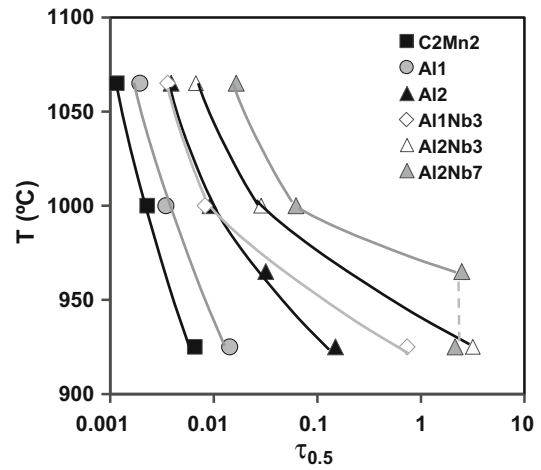

Fig. 7 Normalized time for 50% softening obtained for the steels investigated at the different deformation conditions

than one order of magnitude lower than the levels employed in the present work.

On the other hand, the SRP value obtained for Al is significantly lower than those reported for Nb, V, Mo, or Ti (Ref 34). This agrees well with the small solute retarding effect observed for conventional Al addition levels (Ref 32-35). However, it must be noted that the amount of Al considered in this work is high, far from the typical microalloying contents. For instance, comparing the Al SRP value with that obtained by Jonas et al. (Ref 35) for Nb in Nb steels (222) leads to a retardation effect exerted by 1 and 2 wt.%Al which is equivalent to that exerted by 0.027 and 0.054 wt.%Nb, respectively.

Taking into account the above results the equation proposed by Fernandez et al. (Ref 16) for the time to reach 50% recrystallization was implemented to include the effect of Al in solid solution as follows:

$$t_{0.5SRX} = 9.92 \times 10^{-11} D_0 \epsilon^{-5.6D_0^{-0.15}} \dot{\epsilon}^{-0.53} \exp\left(\frac{180000}{RT}\right)$$
$$\exp\left[\left(\frac{275000}{T} - 185\right) \cdot ([Nb] + 0.374[Ti] + 0.027[Al])\right], \qquad (Eq\ 5)$$

where [Nb], [Ti], and [Al] represent the wt.% concentrations of dissolved Nb, Ti, and Al, respectively. In the calculations, all the Nb content of the steels was considered to be in solution. Figure 8 illustrates the good correlation between experimental data and the values calculated using Eq. (5), including only those data where complete recrystallization is guaranteed, i.e., neither interaction with precipitation nor phase transformation occurs.

Finally, in Fig. 9 the experimental recrystallized grain sizes have been compared to the predictions of the following equations taken from the literature:

$$D_{SRX} = 0.743 D_0^{0.67} \epsilon^{-1}, \qquad (Eq\ 6)$$

$$D_{SRX} = 1.1 D_0^{0.67} \epsilon^{-0.67}, \qquad (Eq\ 7)$$

$$D_{SRX} = 1.4 D_0^{0.56} \epsilon^{-1}. \qquad (Eq\ 8)$$

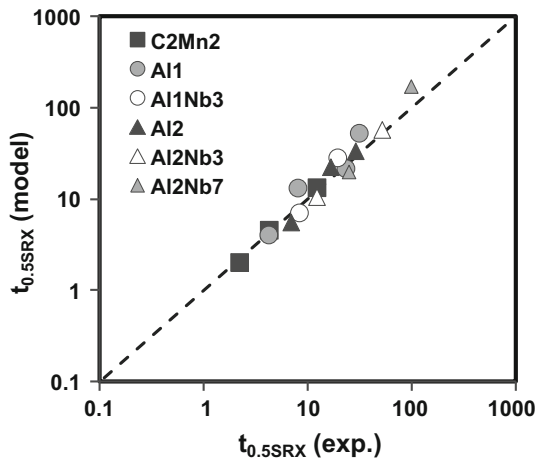Equation (6) was proposed for C-Mn steels (Ref 24), while Eq. (7) (Ref 25) and (8) (Ref 26) were proposed for C-Mn-Nb

Fig. 8 Comparison between $t0.5$ experimental data and the predictions of Eq. (5)

Fig. 9 Comparison between the experimental recrystallized grain size and those calculated by different equations from the literature (Ref 24-26)

steels. It can be observed that independently of steel composition, Eqs. (6) and (7) tend to underestimate the experimentally determined values, the first one for the highest applied strain value ($\varepsilon = 0.35$) and the second one in all the cases. Equation (8) seems to provide the better fit within the range of conditions investigated.

4.2 Strain-Induced Precipitation Kinetics

In the case of the 2%Al steels, at temperatures lower than 1000 °C, a complex interaction between recrystallization, strain-induced precipitation, and phase transformation was observed. As a result, for these steels it is difficult to extract information on the austenite strain-induced precipitation process. Therefore, only the data obtained for the C2Mn1Nb3 and Al1Nb3 steels will be considered for the analysis of the Al effect on strain-induced precipitation kinetics.

As previously shown from the replica analysis in section 3.3.2., although after deformation at 900 and 925 °C similar precipitate sizes were obtained for both steels, at early stages precipitates were clearly more abundant in the Al-free steel. This is an indication of the retardation of the strain-induced precipitation kinetics in Al1Nb3. The reasons for this apparent delay could be attributed to several reasons; on the one hand, the larger Mn content present in this steel (2%) as compared to the C2Mn1Nb3 steel (1%) should be taken into account. The potential of Mn and Al for retarding Nb precipitation has been reported by several authors (Ref 30, 36, 37). In the case of Mn, this effect has been attributed to a reduction in the carbon activity coefficient, whereas for Al the retardation of Nb precipitation is related to the high affinity of Al to N (Ref 38). This agrees also with the results obtained by Wang, who found that the addition of 0.08%Al to a 0.04%Nb-microalloyed steel resulted in a delay on the strain-induced precipitation kinetics by a factor ranging from 1.25 to 2 for temperatures ranging from 900 to 950 °C (Ref 33). It must be remembered that the amount of Al present in the Al1Nb3 steel is an order of magnitude higher than the Al levels considered by Wang. In the case of the Al1Nb3 steel, all the N is expected to be pinned in the form of AlN precipitates; therefore, only NbC strain-induced precipitation can take place in this steel, which is expected to occur at lower temperatures than Nb(C,N) precipitation.
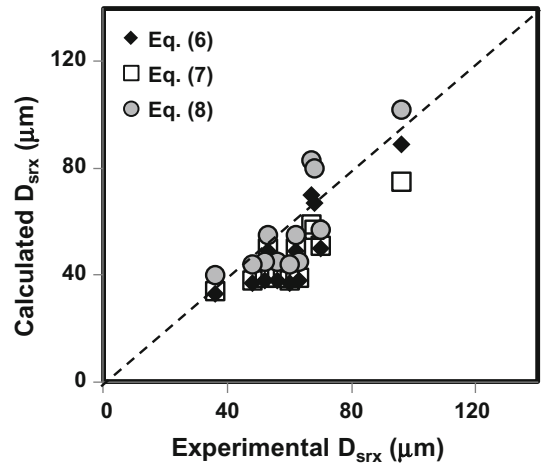
Several authors have related the time for 5% precipitate volume fraction to the time for the *plateau* onset detected from the softening curves. As can be observed from Fig. 1(c), in the case of the softening curves obtained for Al1Nb3 at low temperatures, detecting the time of the plateau onset can be quite complicated. However, the experimental data suggest that this is in the range of $t \sim 100$ s both at 925 and 900 °C. In a previous work, taking into account a large amount of precipitation data reported in the literature, a model for the prediction of strain-induced precipitation start time was developed (Ref 21). The times predicted by this model were $t_{0.05p} = 13$ and 14 s for 925 and 900 °C, respectively, and thus significantly shorter than the experimental values estimated for Al1Nb3. As mentioned above, this apparent delay could be due to various factors. However, due to the limited amount of data, quantification of this effect seems difficult.

4.3 Application to Plate and Strip Hot Rolling Schedules

The softening results obtained above were obtained for single pass and isothermal deformation conditions. However, in order to predict the austenite microstructural evolution during hot rolling, it is necessary to be able to predict the austenite behavior under multipass anisothermal conditions. In a previous work, a thorough model which takes into account the interaction between static recrystallization, grain growth, and strain-induced precipitation and allows the prediction of the austenite microstructure evolution, softening level between deformation passes and the amount of Nb precipitated under multipass deformation conditions was developed for Nb and Nb-Ti-microalloyed steels (Ref 21). For this model to be applied to Al and Al-Nb steels, it was implemented with Eq. (5) in order to take into account the effect of Al on the static softening kinetics, and in view of the results shown in Fig. 8, Eq. (8) was considered for the calculation of the recrystallized grain size.

In order to validate the applicability of the model, multipass torsion tests were carried out at conditions representative of laboratory scale plate and strip hot rolling. The simulation tests were carried out with the Al1Nb3 steel so as to avoid $\gamma \rightarrow \alpha$ phase transformation during the deformation schedule. As mentioned above, for this steel a delay in the strain-induced

precipitation kinetics was also observed. Due to the small amount of available experimental data, this effect was not quantified, and therefore, it should be taken into account that at low temperatures the contribution of strain-induced precipitation could be overestimated, since the effect of Al is not taken into account in the current precipitation model (Ref 21). In a previous work, interrupted multipass torsion tests were performed to analyze the possible contribution of Nb carbides precipitation to recrystallization delay and its effect on the T_{nr} temperature (Ref 11). For all the steels investigated, a very limited number of Nb particles were found in all the samples quenched below the T_{nr} temperature. It was concluded that Al and Nb solute-drag effect was the main mechanism responsible for the T_{nr} increase without interaction with strain-induced precipitation.

The deformation parameters employed in the hot rolling simulations are shown in Tables 5 and 6, for strip and plate, respectively. These were defined according to conventional controlled rolling (CCR) strategies, that is, austenite refinement during the roughing stage by successive cycles of recrystallization, and finishing in the no-recrystallization region in order to obtain a pancaked austenite microstructure. For strip rolling simulation, two sequences with similar thermal cycle and different deformation levels, representative of the production of strips of 6- and 3-mm final gage thicknesses were applied (Table 5) (Ref 39). In the case of plate rolling, in both simulations the deformation applied was similar, and the deformation temperatures of the last deformation passes were varied in order to simulate finishing conditions corresponding to end rolling entry temperatures of 930 and 1040 °C (Table 6)

(Ref 39). It must be mentioned that although the deformation conditions were designed to represent the real laboratory rolling schedules, due to limitations in the torsion machine some modifications had to be performed. These consisted of the application of lower strain rates during the last deformation passes in the strip rolling simulations, and slightly larger strain values in some of the passes of the plate sequences. After the deformation schedule, the torsion specimens were cooled down at 20 °C/s up to 800 °C, followed by water quenching for metallographic analysis.

Figure 10 shows the stress-strain curves obtained in the torsion tests for the above simulations. It can be observed that, due to the larger amount of applied deformation, in the strip deformation sequences (Fig. 10a) the stress levels tend to be larger than in the plate simulations (Fig. 10b). The figure also shows that for the two strip sequences the stress increases continuously as the temperature decreases, the increase rate being larger after the third pass in both. In the case of plate rolling (Fig. 10b), the stress increases significantly after the 4th deformation pass, which corresponds to the finishing rolling simulation start. As expected, this effect is enhanced for the lower end rolling entry temperature case.

From the stress-strain curves, the interpass fractional softening between deformation passes was calculated using the equation proposed by Liu et al. (Ref 31). More details can be found in (Ref 11).

The experimental softening results obtained from all the tests carried out are compared with the model predictions in Fig. 11. For the two strip simulations (Fig. 11a and b), the experimental softening behavior is similar; after the first deformation pass only partial softening takes place, within the second and third interpass times full softening is achieved, and finally, during the last deformation passes low softening levels are obtained in both cases. This indicates that strain accumulation takes places in the last three passes, in good agreement with the higher stress increase observed in the stress-strain curves (Fig. 10a). It can be observed from the figures that the softening behavior is fairly well reproduced by the model. The major deviations are found at the first pass where softening is highly overestimated in both cases. This can be attributed to the relatively low deformation level and high temperature at which the first deformation pass is applied, which is outside the range of deformation conditions the model was developed for (Ref 16, 21). It must be mentioned that according to the model, strain-induced precipitation is not predicted to occur during the
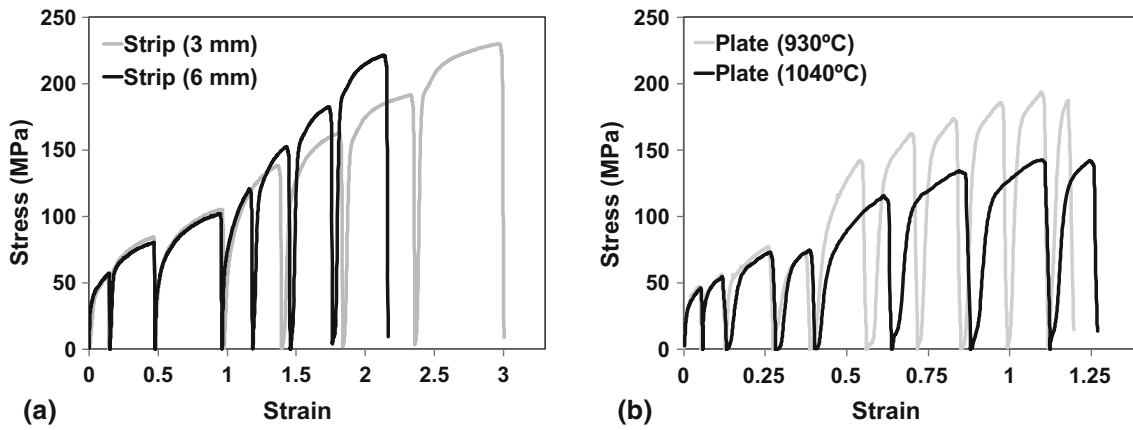
Table 5 Deformation sequences employed in the tests for strip rolling simulation

Pass	900 °C-6 mm				900 °C-3 mm			
	T, °C	ε	$\dot{\varepsilon}$, s^{-1}	t_{ip}, s	T, °C	ε	$\dot{\varepsilon}$, s^{-1}	t_{ip}, s
1	1200	0.15	~1	7.5	1200	0.14	~1	7.5
2	1160	0.33	~1	11.5	1160	0.33	~1	11.5
3	1100	0.48	~1	12	1100	0.50	~1	12
4	1030	0.22	1.69	7	1030	0.42	2.57	7
5	994	0.27	2.02	5.4	994	0.44	2.47	5.4
6	951	0.31	1.96	3.9	951	0.52	2.71	3.9
7	900	0.40	2.27	5	900	0.64	2.72	5

Table 6 Deformation sequences employed in the tests for plate rolling simulation

Pass	930 °C-50 mm				1040 °C-50 mm			
	T, °C	ε	$\dot{\varepsilon}$, s^{-1}	t_{ip}, s	T, °C	ε	$\dot{\varepsilon}$, s^{-1}	t_{ip}, s
1	1200	0.06	1.0	8.5	1200	0.06	1.0	8.5
2	1191	0.07	1.1	29.5	1191	0.10	1.4	29.5
3	1161	0.15	1.7	9.6	1161	0.15	1.8	9.6
4	1149	0.11	1.4	286.9	1149	0.12	1.4	115.5
5	927	0.17	1.8	11.8	1042	0.24	2.2	11.8
6	916	0.16	1.8	12.9	1026	0.24	2.3	13
7	903	0.14	1.7	14	1006	0.24	2.2	14.2
8	889	0.14	1.8	14.1	984	0.15	1.76	10
9	874	0.13	1.7	14.2	...	...	...	...
10	860	0.08	1.4	10	...	...	...	...

Fig. 10 Strain-stress curves obtained in the torsion tests for (a) strip and (b) plate rolling simulation
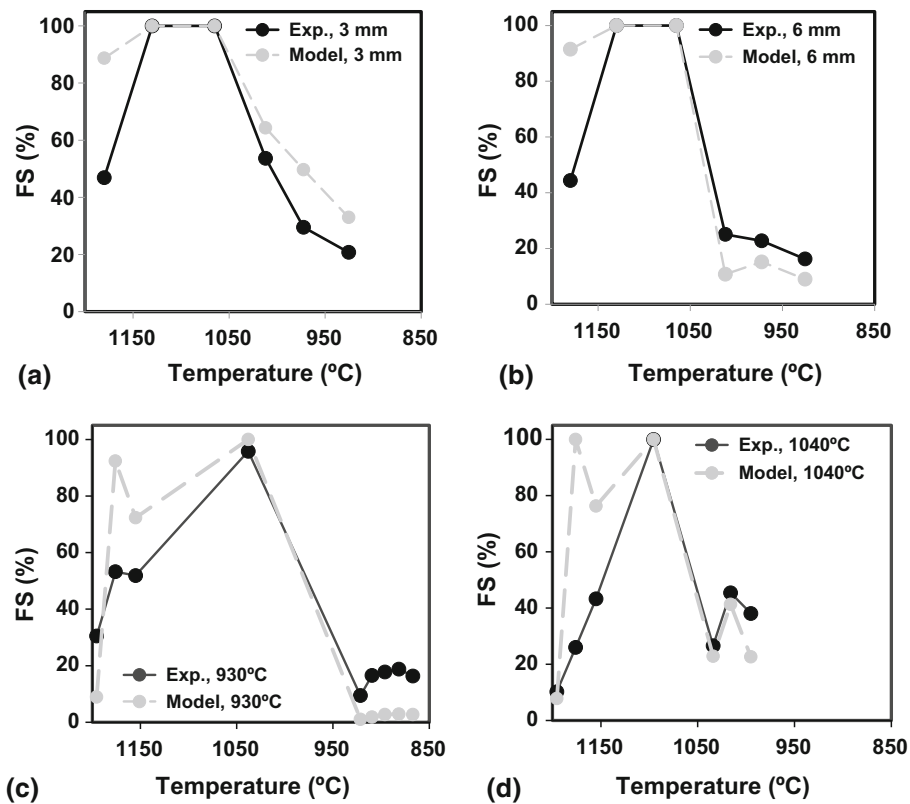

Fig. 11 Comparison between experimental and model-predicted softening for the different rolling simulations

strip deformation sequences. This suggests that in these sequences strain accumulation takes place mainly due to Al and Nb solute-drag retardation effect.

In the case of the plate rolling sequences (Fig. 11c-d), it is interesting to note that during the first deformation passes low experimental softening levels are obtained. Although the temperatures at which these roughing passes are given are high (T = 1200 to 1150 °C), the low softening levels can be attributed to the small amount of deformation applied together with the solute-drag effect exerted by Al and Nb. As in the case of the strip rolling sequences, at these stages the model tends to overestimate the softening. In the two sequences, after the last

roughing pass (4th pass), full softening is achieved. This is due to the large interpass time between the roughing and finishing stages, 285 and 115 s for the 930 and 1040 °C end rolling entry temperatures, respectively. Finally, during finishing, low softening levels are obtained in both sequences, although, as expected, these tend to be slightly larger for the high-temperature simulation. It can also be observed that in these cases the softening evolution is well predicted by the model. In both sequences, strain-induced precipitation is predicted to take place after the 6th pass. Despite the good agreement with the experimental data, it must be remembered that the contribution of strain-induced precipitation could be overestimated by the
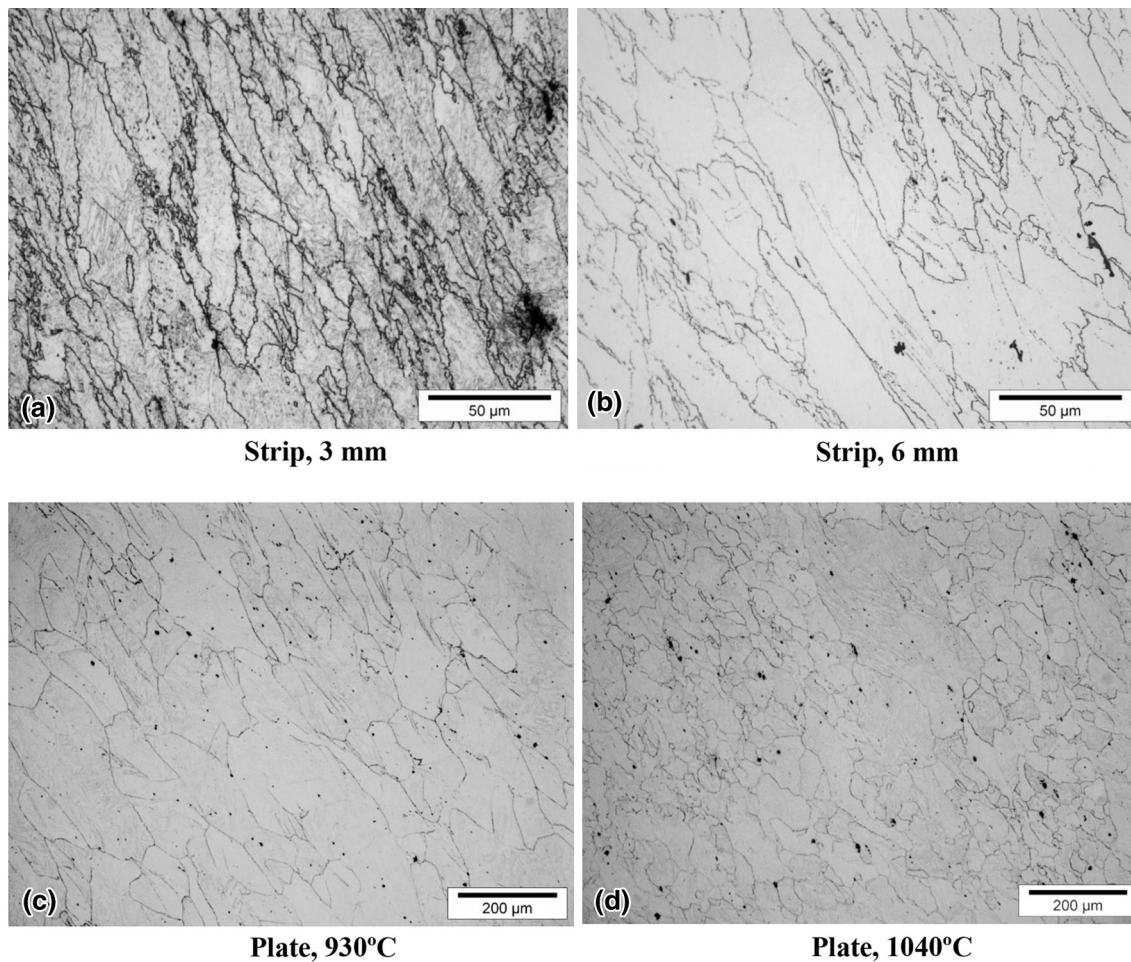
(a) 50 μm	**(b)** 50 μm
Strip, 3 mm	**Strip, 6 mm**
(c) 200 μm	**(d)** 200 μm
Plate, 930ºC	**Plate, 1040ºC**

Fig. 12 Final microstructures obtained after the torsion tests simulating strip and plate rolling conditions

model, since the possible retardation effect of Al on precipitation kinetics is not considered in the calculations. As shown in the figure, after the 5th deformation pass a very low experimental softening level is also observed, which is also well reproduced by the model. This would indicate that in the absence of strain-induced precipitation, the temperature drop in the finishing passes in combination with Al and Nb solute-drag effect could also explain the low softening levels observed.

Figure 12 shows micrographs corresponding to the microstructures of the torsion specimens quenched after the different rolling simulations. In good agreement with the results shown above, in all the cases the microstructures denote a certain strain accumulation level. Nevertheless, the microstructures obtained after plate rolling simulations (Fig. 12c and d) are significantly coarser and have a more equiaxed shape than those found after strip rolling (Fig. 12a and b). Within the strip rolling sequences, the microstructure obtained in the 3 mm simulation is finer and shows a higher degree of strain accumulation than the 6 mm one. In the case of the plate schedules, the microstructure obtained after the higher temperature simulation is clearly refined and more equiaxed. In this case the higher temperatures and larger strains applied during finishing in the 1040 °C end rolling entry temperature simulation allow a major degree of recrystallization and finer recrystallized grain sizes to be achieved, compared to the other sequence where the strains and temperatures applied during finishing are lower and as a result recrystallization is nearly avoided.

It should be noted that in the case of higher finishing temperatures a major degree of microstructural heterogeneity, which is associated with partial recrystallization, is also observed. The presence after roughing of some isolated coarse grains that remain unrecrystallized and appear elongated in the final microstructure is clearly evident in Fig. 12(d).

In order to compare the results obtained with the model predictions, the deformed microstructures shown above were characterized. In this case, in addition to the equivalent diameter (EQD), the average grain size measured by linear intersection (MLI) was calculated, using a circular grid. The results obtained together with the model predictions are shown in Fig. 13. In Fig. 13(b), the grain size measurements taken for a sample quenched after the 4th pass (representing the roughing state) in an interrupted test corresponding to 1040 °C end rolling entry temperature condition have been also included for comparison.

It can be observed that the grain sizes measured using both procedures are quite similar in most cases. It can also be noted that in all the cases the model gives a good approximation of the final austenite grain size. In contrast, for the test interrupted after the 4th pass in plate simulations, the model clearly overestimates the grain size, following the same tendency observed for the predictions at initial passes. For an initial grain size of ∼100 μm, the model predicts an increase of the grain size up to values larger than 300 μm, which seems to be quite unrealistic. This means that similar to the predictions of
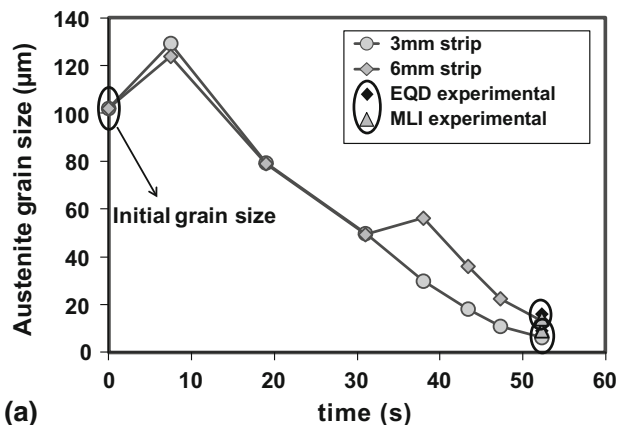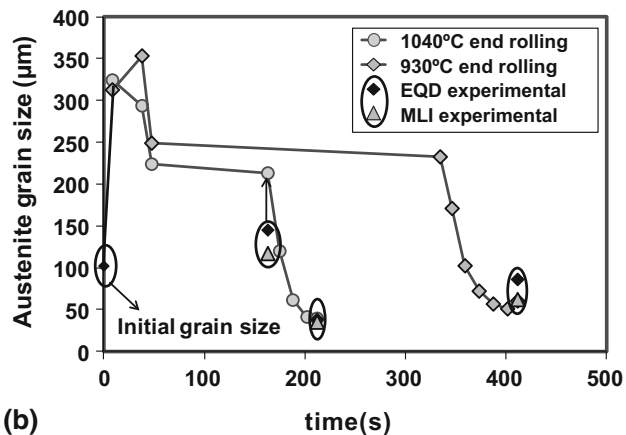
Fig. 13 Comparison between experimental measurements and model predictions for the evolution of austenite grain size during rolling simulations for (a) strip; (b) plate. The represented grain size is the one calculated at the end of each interpass interval

fractional softening, which were overestimated at low strains, the accuracy of the predictions for the recrystallized grain size at these conditions is poor. Current investigations are now underway in order to improve both the softening and recrystallized grain size predictions for these low-strain conditions.

5. Conclusions

– 1%Al addition to a CMn steel retards the softening kinetics due to the solute-drag effect at all the temperatures investigated, equivalent to that exerted by 0.027%Nb. However, for the 2%Al steel at temperatures lower than 1000 °C, γ → a phase transformation takes place after deformation, resulting in enhanced retardation of the softening kinetics.

– At temperatures higher than 1000 °C, Nb addition to the high Al steels also contributes to the retardation of the softening kinetics due to solute-drag effect. At lower temperatures, NbC strain-induced precipitation takes place and results in incomplete softening for the 1%Al steel and in a complex interaction between recrystallization, strain-induced precipitation, and phase transformation for the 2%Al steels.

– The effect of Al in solid solution on the static softening kinetics was quantified and implemented in a pre-existing model for the prediction of the austenite microstructure evolution under multipass anisothermal conditions.

– Torsion tests were carried out at conditions representative of strip and plate hot rolling. Although the results of the model are in good agreement with the experimental softening and austenite microstructure in a wide range of deformation and temperature conditions, the model fails in the case where low deformations are applied.

References

1. M. Gómez, C.I. García, D.M. Haezebrouck, and A.J. Deardo, Design of Composition in (Al/Si)-Alloyed TRIP Steels, *ISIJ Int.*, 2009, **49**(2), p 302–311
2. C. Georges, S. Godet, and P.J. Jaques, Development of High Perfomance Nb-Added Hot Rolled Bainitic Steels Presenting a TRIP Effect, *Mater. Sci. Forum*, 2005, **500–501**, p 437–444
3. P.J. Jacques, E. Girault, A. Mertens, B. Verlinden, J. van Huumbeeck, and F. Delannay, The Developments of Cold-Rolled TRIP-Assisted Multiphase Steels, Al-Alloyed TRIP Assisted Multiphase Steels, *ISIJ Int.*, 2001, **41**(9), p 1068–1074
4. A.K. Srivastava, D. Bhattacharjee, G. Jha, N. Gope, and S.B. Singh, Microstructural and Mechanical Characterization of C-Mn-Al-Si Cold-Rolled TRIP-Aided Steel, *Mater. Sci. Eng. A*, 2007, **445–446**, p 549–557
5. E. Girault, A. Merterns, P. Jacques, Y. Houbaert, B. Verlinden, and J. Van Humbeeck, Comparison of the Effects of Silicon and Aluminium on the Tensile Behaviour of Multiphase TRIP-Assisted Steels, *Scripta Mater.*, 2001, **44**(6), p 885–892
6. D.Q. Bai, A. Di Chiro, and S. Yue, Stability of Retained Austenite in a Nb Microalloyed Mn-Si TRIP Steel, *Mater. Sci. Forum*, 1998, **284–286**, p 253–260
7. Z. Li and D. Wu, Effects of Hot Deformation and Subsequent Austempering on the Mechanical Properties of Si-Mn TRIP Steels, *ISIJ Int.*, 2006, **46**(1), p 121–128
8. E.I. Poliak and F. Siciliano, *Hot Deformation of Mn-Al and Mn-Al-Nb Steels, 2004 MS&T Conference Proceedings, 2004 (Lousiana)*, The Minerals, Metals and Materials Society (TMS), Association for Iron & Steel Technology (AIST), 2004, p 39–45
9. P.P. Suikkanen, V.T.E. Lang, M.C. Somani, D.A. Porter, and L.P. Karjalainen, Effect of Silicon and Aluminium on Austenite Static Recrystallization Kinetics in High-Strength TRIP-aided Steels, *ISIJ Int.*, 2012, **52**(3), p 471–476
10. Z. Aretxabaleta, B. Pereda, and B. López, Analysis of the Effect of Al on the Static Softening Kinetics of C-Mn Steels Using a Physically Based Model, *Metall. Mater. Trans.*, 2014, **45A**(2), p 934–947
11. Z. Aretxabaleta, B. Pereda, and B. López, Multipass Hot Deformation Behaviour of High Al and Al-Nb Steels, *Mater. Sci. Eng. A*, 2014, **600**, p 37–46
12. M. De Meyer, D. Vanderschueren, and B.C. DeCooman, The Influence of the Substitution of Si by Al on the Properties of Cold Rolled C-Mn-Si TRIP Steels, *ISIJ Int.*, 1999, **39**(8), p 813–822
13. A. Fernandez, B. Lopez, and J.M. Rodriguez-Ibabe, Relationship Between the Austenite Recrystallised Fraction and the Softening Measured from the Interrupted Torsión Test Technique, *Scr. Mater.*, 1999, **4**(5), p 543–549
14. F.J. Humphreys and M. Hatherly, *Recrystallisation and Related Annealing Phenomena*, 2nd ed., Elsevier, Amsterdam, 2004, p 229–232

15. S.F. Medina, A. Quispe, P. Valles, and J.L. Banos, Recrystallization-Precipitation Interaction Study of Two Medium Carbon Niobium Microalloyed Steels, *ISIJ Int.*, 1999, **39**(9), p 913–922

16. A.I. Fernandez, P. Uranga, B. López, and J.M. Rodríguez-Ibabe, Static Recrystallization Behaviour of a Wide Range of Austenite Grain Sizes in Microalloyed Steels, *ISIJ Int.*, 2000, **40**(9), p 893–901

17. F. Siciliano and E.I. Poliak, Modeling of the Resistance to Hot Deformation and the Effects of Microalloying in High-Al Steels under Industrial Conditions, *Mater. Sci. Forum*, 2005, **500–501**, p 195–202

18. Thermodynamic Database TCFE6-TCS Steels/Fe-Alloys Database, Thermo-Calc

19. J.O. Andersson, T. Helander, L. Höglund, P. Shi, and B. Sundman, Thermo-Calc & DICTRA, Computational Tools for Materials Science, *CALPHAD*, 2002, **26**(2), p 273–312

20. D.Q. Bai, S. Yue, W.P. Sun, and J.J. Jonas, Effect of Deformation Parameters on the No-Recrystallization Temperature in Nb-Bearing Steels, *Metall. Mater. Trans.*, 1993, **A24**(10), p 2151–2159

21. B. Pereda, J.M. Rodríguez-Ibabe, and B. López, Improved Model of Kinetics of Strain Induced Precipitation and Microstructure Evolution of Nb Microalloyed Steels during Multipass Rolling, *ISIJ Int.*, 2008, **48**(10), p 1457–1466

22. J. Irvine, F.B. Pickering, and T. Gladman, Grain Refined C-Mn Steels, *J. Iron Steel Inst.*, 1967, **205**, p 161–182

23. S. Koyama, T. Ishii, and K. Narita, Effects of Mn, Si, Cr and Ni on the Solution and Precipitation of Niobioum Carbide in Iron Austenite, *J. Jpn. Inst. Met.*, 1971, p 1089–1094

24. J.H. Beynon and C.M. Sellars, Modelling Microstructure and Its Effects During Multipass Hot Rolling, *ISIJ Int.*, 1992, **32**(3), p 359–367

25. C.M. Sellars, The Physical Metallurgy of Hot Working, Hot Working and Forming Processes, *Proceedings of An International Conference*, 1979, ed. By C.M. Sellars and G.J. Davies, 1979 (Sheffield), Met. Soc., London, 1980, p. 3–15

26. R. Abad, A.I. Fernández, B. López, and J.M. Rodríguez-Ibabe, Interaction between Recrystallization and Precipitation During Multipass Rolling in a Low Carbon Niobium Microalloyed Steel, *ISIJ Int.*, 2001, **41**(11), p 1373–1382

27. A. Laasraoui and J.J. Jonas, Recrystallization of Austenite After Deformation at High Temperatures and Strain Rates-Analysis and Modeling, *Metall. Trans.*, 1991, **22A**(1), p 151–160

28. P.D. Hodgson and R.K. Gibbs, A Mathematical Model to Predict the Mechanical Properties of Hot Rolled C-Mn and Microalloyed Steels, *ISIJ Int.*, 1992, **3**(12), p 1329–1338

29. S.F. Medina and A. Quispe, Improved Model for Static Recrystallization Kinetcis of Hot Deformed Austenite in Low Alloy and Nb/V Microalloyed Steels, *ISIJ Int.*, 2001, **41**(7), p 774–781

30. A. Grajcar, P. Skrzypczyk, R. Kuziak, and K. Golombek, Effect of Finishing Hot-Working Temperature on Microstructure of Thermomechanically Processed Mn-Al Multiphase Steels, *Steel Res. Int.*, 2014, **85**(6), p 1058–1069

31. W.J. Liu and M.G. Akben, Softening Behavior or Two Ti Bearing Steels During Torsional Simulation of Rolling, *Can. Metall. Q.*, 1987, **26**(2), p 145–153

32. H.J. McQueen, S. Yue, N.D. Ryan, and E. Fry, Hot Working Characteristics of Steels in Austenitic State, *J. Mater. Process. Technol.*, 1995, **53**, p 293–310

33. G. Wang, "*Static Recrystallization and Precipitation in Nb-Al HSLA Steels*", PhD Thesis, McGill University, Montreal, Canada, 1990

34. J. Jonas, *Mechanical Testing for the Study of Austenite Recrystallization and Carbonitride Precipitation, High Strength Low Alloy Steels Proc.*, D.P. Dunne and T. Chandra, Eds., University Press, Wollongong, 1984, p 80–91

35. J.P. Michel and J.J. Jonas, Precipitation Kinetics and Solute Strengthening in High Temperature Austenite Containing Al and N, *Acta Metall.*, 1980, **29**(3), p 513–526

36. M.G. Akben, T. Chandra, P. Plassiard, and J.J. Jonas, Dynamic precipitation and solute hardening in a titanium microalloyed steel containing three levels of manganese, *Acta Metall.*, 1984, **32**(4), p 591–601

37. F. Siciliano, Jr, and J.J. Jonas, Mathematical Modeling of the Hot Strip Rolling of Microalloyed Nb, Multiply-Alloyed Cr-Mo, and Plain C-Mn Steels, *Metall. Trans.*, 2000, **31A**(2), p 511–530

38. R.M. Skolly and E.I. Poliak, Aspects of Production Hot Rolling of Nb Microalloyed High Al High Strength Steels, *Mater. Sci. Forum*, 2005, **500–501**, p 187–194

39. S.V. Parker, R.C. Beaverstock, Z. Husain, G. Claxton, S. Cobo, L. Lutz, S. Joly, Z. Aretxabaleta, B. Pereda, B. López, B. Pohu and G. Lanno, *Development of Microstructure Based Tools for Alloy and Rolling Process Design (Microtools)*, Final Report, Eur 26212, Luxembourg (2013)